Acta Crystallographica Section A
Foundations of Crystallography
ISSN 0108-7673

Received 7 May 2001
Accepted 6 June 2002

Can a multipole analysis faithfully reproduce topological descriptors of a total charge density?

Ian Bytheway, Graham S. Chandler* and Brian N. Figgis

School of Biomedical and Chemical Sciences, Faculty of Life and Physical Sciences, University of Western Australia, 35 Stirling Hwy, Crawley, WA 6009, Australia. Correspondence e-mail: gsc@crystal.uwa.edu.au

Total charge densities $\rho(\mathbf{r})$ of solid NH_3 have been derived using an *ab initio* crystalline molecular-orbital approach and also from multipole refinement of the structure factors obtained from the same charge density. Comparison of the topological features of these charge densities, as defined by the quantum theory of atoms in molecules, has been used to probe the ability of the multipole analysis to reproduce exactly known total charge-density distributions. For the most part, multipole refinement satisfactorily returns the features of the original density, although the fit to theoretical data is not as good as that to the experimental data. The one topological parameter that is poorly reproduced is the Laplacian $\nabla^2\rho(\mathbf{r}_b)$ at NH bond critical points.

1. Introduction

The fitting of multipolar density functions to experimental X-ray diffraction data has become a standard method of obtaining experimental electron densities (Coppens, 1997; Koritsánszky & Coppens, 2001). The model of expanding the charge density of a molecule in a unit cell through a finite expansion of multipoles centred on each atomic centre was first proposed by Dawson (1967). It was further elaborated by Stewart *et al.* (Stewart, 1976; Bentley & Stewart, 1976; Epstein *et al.*, 1977). Electron densities expressed in this manner can be used to obtain molecular electronic properties such as orbital populations, deformation densities and electrostatic moments (Coppens, 1992; Koritsánszky & Coppens, 2001). The topology of such densities can also be analysed using the theory of atoms in molecules (AIM) (Bader, 1990). A variety of such studies has been published, ranging from the relatively simple NH_3 molecule (Boese *et al.*, 1997) to more complex organic molecules (Flaig *et al.*, 1998; Souhassou & Blessing, 1999; Koritsánszky *et al.*, 1999, 2000), and transition-metal complexes (Smith *et al.*, 1997; Iversen *et al.*, 1997; Macchi *et al.*, 1998*a*,*b*; Bianchi *et al.*, 2000; Bytheway *et al.*, 2001) as well as the bulk crystalline phase of SiO_2 (Rosso *et al.*, 1999) and Cu_2O (Lippmann & Schneider, 2000). Analysis of charge densities using the theory of AIM is appealing since it provides definitions of atoms and bonds that depend only on the charge density, not upon the method by which it was obtained. Direct comparison with theoretical charge densities is, therefore, straightforward.

In general, the agreement of topological descriptors of the charge density obtained from multipole-fitted experimental charge densities with those obtained from *ab initio* molecular-orbital calculations is not particularly close unless the theoretical density also is projected into a multipolar expansion (Howard *et al.*, 1992, 1995; Volkov, Abramov, Coppens & Gatti, 2000; Volkov, Gatti, Abramov & Coppens, 2000). One possible contribution to this disagreement between experimental densities obtained through a multipole expansion and those obtained directly from theory is the multipole analysis itself. This paper is solely concerned with assessing the accuracy with which the currently favoured multipole models can reproduce a precisely known density in a crystal.

The approach used in this work is similar in spirit to that of Spackman *et al.* (Spackman & Byrom, 1996; Spackman *et al.*, 1999). In their work, structure factors were calculated by *ab initio* methods for crystalline systems and then subjected to aspherical atom multipole refinement. Multipole functions were used to compute molecular dipole moments, quadrupole and second moments, interaction energies and electric field gradients at each nuclear site, all of which were compared with results obtained from the original *ab initio* wavefunctions. Volkov, Abramov, Coppens & Gatti (2000) used the methods employed here as part of their consideration of the discrepancies between experiment and theory for the properties of bond critical points in *p*-nitroaniline and *p*-amino-*p*′-nitrobiphenyl.

Investigations of the multipole analysis of charge densities in molecules have also appeared recently. de Vries *et al.* (2000) have calculated structure-factor amplitudes for urea and subjected them to multipole analysis in order to test the reliability of this approach for obtaining interaction densities. Moss *et al.* (1995) used simulated X-ray data obtained from single-molecule HF calculations on H_3PO_4 to test pseudoatom multipole modelling of the valence-electron-density distribution. Specifically, these authors were interested in the radial modelling of the *M* valence shell of phosphorus, and in the

deconvolution of nonspherical density features from anisotropic vibrational smearing. In a recent study by Pérès *et al.* (1999), it has been shown that a number of different multipole expansions fit the experimental X-ray data for ammonium dihydrogen phosphate equally well. Another study, by Pillet *et al.* (2001), was directly concerned with the capability of the multipole model to reproduce the electron density of corundum. Theoretical as well as experimental data were used. Complete fitting of the data for this crystal required an extension of the standard multipole model to include both a core κ parameter and multipoles up to $l_{\max} = 6$. In a different vein, Volkov *et al.* (2001) used multipole refinement of theoretical structure factors to obtain optimized values of the κ' parameters that govern the expansion or contraction of the radial functions in the higher multipole expressions. Their purpose was to confirm the correlation between monopole-derived net atomic charges and atomic κ' values and establish a relation between the two that could be useful in multipole refinements of X-ray data for large molecules.

In contrast, we have used a much simpler model system, crystalline NH_3, in order to examine carefully the ability of the multipole method in its standard form to reproduce a precisely known charge density. The NH_3 crystal has been the subject of a recent X-ray diffraction experiment (Boese *et al.*, 1997) and was chosen for this work in order to take advantage of the known crystal parameters.

The purpose of this paper, therefore, is to compare the topological descriptors obtained from a precisely known charge-density distribution derived from an *ab initio* calculation with those obtained from a multipole analysis of the structure factors generated from the same *ab initio* charge density. This was carried out by focusing upon the topology of the total charge density $\rho(\mathbf{r})$ and the negative of its Laplacian $[L = -\nabla^2\rho(\mathbf{r})]$.

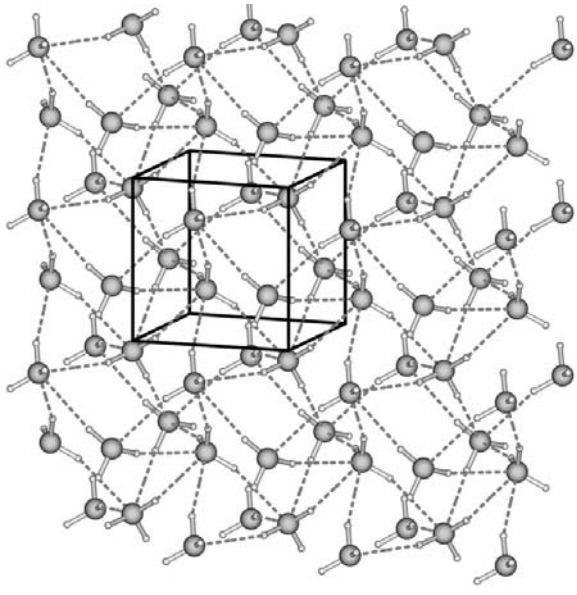

Figure 1
The experimental structure of NH_3. The space group is $P2_13$ with a = 5.1305, d(N—H) = 1.01, d(N···H) = 2.400 Å and ∠H—N—H = 109.0°.

2. Theoretical details

Total charge densities, $\rho(\mathbf{r})$, and X-ray structure factors, $F_{\rm CMO}$, for crystalline NH_3 were calculated using the crystalline molecular orbital (CMO) approach of the *CRYSTAL98* software package (Saunders *et al.*, 1998). Cell parameters from the experimental study of NH_3 (Boese *et al.*, 1997) were used throughout. Fig. 1 shows the relative arrangement and geometries of NH_3 molecules in a unit cell. The conventional Hartree–Fock method as well as the BLYP density-functional method (Becke, 1988; Lee *et al.*, 1988) were used to generate total charge densities. The *TOPOND* program (Gatti, 1998) was used to analyse the topology of the total charge densities of crystalline NH_3.

The 6-311G** basis set was used (Krishnan *et al.*, 1980) but with the most diffuse *s* and *p* functions removed as recommended (Dovesi *et al.*, 1996) in order to avoid linear dependencies that may arise from the use of very diffuse components and which cause convergence difficulties in the CMO calculations.

The $F_{\rm CMO}$ were used in aspherical atom multipole refinements employing the Hansen–Coppens multipole formalism (Coppens, 1997), as implemented in the *XD* software (Koritsánszky *et al.*, 1997). Within this formalism, the aspherical charge density is described by core, valence and deformation terms in the form of a nucleus-centred multipole expansion:

$$\rho_k(\mathbf{r}) = P_c\rho_c(r) + P_v\kappa^3\rho_v(\kappa r) + \kappa'^3\sum_{l=0}^{4} R_l(\kappa' r)\sum_{m=0}^{l} P_{lm\pm}y_{lm\pm}(\mathbf{r}/r),$$

where ρ_c and ρ_v are the spherically averaged charge densities obtained from a Hartree–Fock wavefunction expanded over Slater-type atomic orbitals (Clementi & Roetti, 1974) and normalized to one electron. The real spherical harmonic angular functions are denoted $y_{lm\pm}$ and R_l for nitrogen are the normalized radial functions obtained from the one-exponent wavefunctions of Clementi & Raimondi (1963) as used by *XD* (Koritsánszky *et al.*, 1997). For hydrogen, both the atomic radial function and the scattering factors of Stewart *et al.* (1965) were employed and the results are compared. The radial extents of the spherical and aspherical densities are controlled by the dimensionless parameters κ and κ', and P_v and $P_{lm\pm}$ are the populations of the different multipoles.

The weighting scheme used during refinement was $w = \sigma^{-2}(F_i^{\rm obs})$, where $F_i^{\rm obs}$ are the structure factors from experiment or from a CMO calculation, and electroneutrality of the NH_3 molecule was enforced. Each structure factor was either assigned a token error $[\sigma(F_i^{\rm obs}) = 0.001]$ or an error based on the experimental errors of Boese *et al.* (1997). Experimental data were kindly supplied by Professor Boese. However, these data were only for reflections with $(\sin\theta/\lambda) < 0.7$ Å^{-1}. σ for these reflections were set at the experimental values while values for those with $0.7 < (\sin\theta/\lambda) \leq 1.05$ Å^{-1} were assigned on the basis of errors for similar intensity reflections in the low-angle experimental data.

Table 1
R-factor agreement statistics, κ(N) and κ'(N) for *XD* refinements.

See the text for details of the abbreviations.

Data	$\%R_f$	κ(N)	κ'(N)	Data	$\%R_f$	κ(N)	κ'(N)
HF(*L*,*W*)	2.46	1.03	1.08	BLYP(*L*,*W*)	2.36	1.02	1.08
HF(*L*,*U*)	2.05	1.03	1.13	BLYP(*L*,*U*)	1.91	1.03	1.15
HF(*A*,*W*)	1.90	1.01	1.06	BLYP(*A*,*W*)	1.78	1.02	1.06
HF(*A*,*W*,*S*)	1.95	1.00	1.08	BLYP(*A*,*W*,*S*)	1.77	1.01	1.10
HF(*A*,*U*)	1.67	1.02	1.09	BLYP(*A*,*U*)	1.49	1.02	1.10
HF(*A*,*U*,*S*)	1.79	1.01	1.10	BLYP(*A*,*U*,*S*)	1.58	1.01	1.12
HF(*A*,*U*,*D*)	1.87	1.02	1.08	BLYP(*A*,*U*,*D*)	1.74	1.02	1.07
HF(6-21G**,*A*,*U*)	0.99	0.98	0.99	EXP(*A*,*U*,*D*)	0.87	0.96	1.00

Table 2
Multipole population parameters from the *XD* refinements.

Parameters for N Data	*M*0	*D*10	*D*20	*O*30	*O*33	*O*3−3	*Q*40	*Q*43	*Q*4−3
HF(*L*,*W*)	7.00 (6)	0.11 (1)	0.10 (1)	−0.02 (1)	0.07 (1)	0.03 (1)	0.00 (1)	−0.01 (1)	0.00 (1)
HF(*L*,*U*)	6.92 (9)	0.10 (1)	0.10 (1)	−0.03 (6)	0.05 (2)	0.05 (6)	0.01 (1)	0.00 (2)	0.00 (2)
HF(*A*,*W*)	7.01 (6)	0.11 (1)	0.10 (1)	−0.01 (1)	0.06 (1)	0.03 (1)	0.00 (1)	−0.01 (1)	0.00 (1)
HF(*A*,*W*,*S*)	7.43 (6)	0.10 (1)	0.10 (1)	0.00 (1)	0.06 (1)	0.04 (1)	0.01 (1)	0.01 (1)	−0.01 (1)
HF(*A*,*U*)	7.01 (6)	0.11 (1)	0.10 (1)	−0.02 (1)	0.05 (1)	0.04 (1)	0.01 (1)	0.00 (1)	0.00 (1)
HF(*A*,*U*,*S*)	7.43 (6)	0.10 (1)	0.10 (1)	−0.01 (1)	0.05 (1)	0.04 (1)	0.01 (1)	0.01 (1)	0.00 (1)
HF(*A*,*U*,*D*)	7.13 (3)	0.09 (1)	0.10 (1)	−0.01 (1)	0.05 (1)	0.04 (1)	0.00 (1)	−0.02 (1)	0.01 (1)
HF(6-21G**,*A*,*U*)	7.31 (3)	0.03 (1)	0.04 (1)	0.00 (1)	0.04 (1)	0.04 (1)	0.01 (1)	−0.01 (1)	0.00 (1)
BLYP(*L*,*W*)	7.13 (9)	0.06 (1)	0.08 (1)	−0.02 (2)	0.06 (1)	0.01 (1)	0.00 (1)	−0.01 (1)	0.00 (1)
BLYP(*L*,*U*)	7.04 (9)	0.06 (1)	0.08 (1)	−0.03 (1)	0.04 (1)	0.04 (1)	0.01 (1)	0.00 (2)	0.00 (1)
BLYP(*A*,*W*)	7.16 (6)	0.07 (1)	0.08 (1)	−0.02 (1)	0.06 (1)	0.02 (1)	0.00 (1)	−0.01 (1)	0.00 (1)
BLYP(*A*,*W*,*S*)	7.55 (3)	0.06 (1)	0.08 (1)	−0.01 (1)	0.06 (1)	0.03 (1)	0.01 (1)	0.01 (1)	0.00 (1)
BLYP(*A*,*U*)	7.16 (6)	0.06 (1)	0.08 (1)	−0.02 (1)	0.04 (1)	0.03 (1)	0.00 (1)	0.00 (1)	0.00 (1)
BLYP(*A*,*U*,*S*)	7.55 (3)	0.05 (1)	0.08 (1)	-0.01 (1)	0.05 (1)	0.03 (1)	0.01 (1)	0.01 (1)	0.00 (1)
BLYP(*A*,*U*,*D*)	7.25 (3)	0.05 (1)	0.08 (1)	−0.01 (1)	0.05 (1)	0.03 (1)	0.00 (1)	−0.02 (1)	0.01 (1)
EXP(*L*,*W*,*D*)	7.55 (3)	0.01 (1)	0.00 (1)	0.02 (1)	0.01 (1)	0.00 (1)	0.00 (1)	0.00 (1)	0.00 (1)

Parameters for H Data	*M*0	*D*11	*D*1−1	*D*10	*Q*20	*Q*21	*Q*2-1	*Q*22	*Q*2−2
HF(*L*,*W*)	1.01 (2)	−0.01 (2)	0.01 (3)	0.17 (2)	0.09 (3)	−0.02 (2)	0.01 (5)	0.00 (3)	0.03 (3)
HF(*L*,*U*)	1.02 (3)	−0.03 (2)	0.02 (4)	0.23 (2)	0.10 (3)	−0.04 (3)	−0.02 (6)	0.05 (3)	0.04 (3)
HF(*A*,*W*)	1.00 (2)	−0.01 (1)	0.00 (2)	0.17 (2)	0.10 (2)	−0.02 (2)	−0.01 (3)	0.01 (2)	0.03 (2)
HF(*A*,*W*,*S*)	0.85 (2)	−0.02 (1)	−0.01 (2)	0.15 (2)	0.05 (2)	−0.03 (2)	−0.04 (3)	0.01 (2)	0.03 (2)
HF(*A*,*U*)	1.00 (2)	−0.03 (1)	0.03 (2)	0.23 (1)	0.09 (2)	−0.04 (2)	−0.02 (3)	0.05 (2)	0.05 (2)
HF(*A*,*U*,*S*)	0.85 (2)	−0.03 (1)	0.02 (2)	0.18 (1)	0.03 (2)	−0.04 (2)	−0.02 (3)	0.05 (2)	0.04 (2)
HF(*H*,*U*,*D*)	0.96 (1)	−0.01 (1)	0.03 (2)	0.23 (1)					
HF(6-21G**,*A*,*U*)	0.90 (1)	0.00 (1)	0.00 (1)	0.16 (1)	0.04 (1)	0.01 (1)	0.00 (1)	0.01 (1)	0.00 (1)
BLYP(*L*,*W*)	0.96 (3)	0.00 (2)	0.03 (4)	0.14 (3)	0.08 (3)	−0.02 (3)	0.03 (5)	0.01 (3)	0.03 (3)
BLYP(*L*,*U*)	0.98 (3)	−0.02 (2)	0.03 (3)	0.21 (2)	0.09 (3)	−0.04 (3)	−0.01 (5)	0.05 (3)	0.04 (3)
BLYP(*A*,*W*)	0.95 (2)	0.00 (1)	0.01 (2)	0.14 (1)	0.09 (2)	−0.01 (2)	0.01 (3)	0.01 (2)	0.04 (2)
BLYP(*A*,*W*,*S*)	0.82 (1)	−0.01 (1)	0.00 (2)	0.13 (2)	0.04 (2)	−0.02 (2)	−0.02 (3)	0.02 (2)	0.03 (2)
BLYP(*A*,*U*)	0.95 (2)	−0.02 (1)	0.03 (2)	0.21 (1)	0.08 (2)	−0.03 (2)	−0.02 (3)	0.07 (2)	0.06 (2)
BLYP(*A*,*U*,*S*)	0.81 (1)	−0.02 (1)	0.02 (2)	0.16 (1)	0.02 (2)	−0.04 (2)	−0.01 (3)	0.06 (2)	0.05 (2)
BLYP(*A*,*U*,*D*)	0.92 (1)	−0.01 (1)	0.03 (2)	0.20 (1)					
EXP(*L*,*W*,*D*)	0.82 (1)	−0.03 (1)	0.00 (1)	0.02 (1)					

Only unique reflections were refined, and no correction for thermal motion was introduced. Refinements were carried out with multipoles for $l \leq 4$ on N (*M*1, *D*0, *Q*0, *O*0, *O*±3, *H*0, *H*±3), and both $l \leq 1$ and $l \leq 2$ on H (*M*1, *D*0, *D*±1) and (*M*1, *D*0, *D*±1, *Q*0, *Q*±1, *Q*±2). The refinement was performed in the following steps:

(i) Refine P_v
(ii) Refine P_{lm}
(iii) Refine P_v and P_{lm}
(iv) Refine κ(N)
(v) Refine κ'(N)
(vi) Refine κ(N) and κ'(N)
(vii) Refine P_v and P_{lm} again.

The κ and κ' values for hydrogen were fixed at 1.2 for the atomic radial functions and at 1.16 (Pérès *et al.*, 1999) for the Stewart *et al.* (1965) functions. This refinement strategy is based on the unrestricted multipole refinement methodology used in recent similar studies (Abramov *et al.*, 1999; Volkov,

Table 3
Bond critical-point parameters for the N—H and N···H bonds from the CMO and *XD* charge densities.

$\rho(\mathbf{r}_b)$ (e Å^{-3}) and $-\nabla^2\rho(\mathbf{r}_b)$ (e Å^{-5}) are the values of the charge density and its Laplacian at the bond critical point; d(N) and d(H) are the distances from the nuclei to the bond critical point (Å); λ_3 is the value of the positive eigenvalue for the N···H bond (e Å^{-5}).

	N—H bond				N···H bond				
Data	$\rho(\mathbf{r}_b)$	$-\nabla^2\rho(\mathbf{r}_b)$	d(N)	d(H)	$\rho(\mathbf{r}_b)$	$-\nabla^2\rho(\mathbf{r}_b)$	λ_3	d(N)	d(H)
HF(CMO)	2.43	49.07	0.704	0.305	0.04	0.96	1.23	1.356	1.082
HF(*L*,*W*)	2.25 (8)	22.2 (4)	0.690	0.321	0.08 (2)	0.80 (2)	1.52	1.464	0.934
HF(*L*,*U*)	2.28 (1)	20.4 (5)	0.675	0.337	0.07 (2)	0.64 (1)	1.31	1.494	0.922
HF(*A*,*W*)	2.24 (6)	22.2 (3)	0.688	0.323	0.08 (2)	0.78 (1)	1.53	1.468	0.931
HF(*A*,*W*,S)	2.02 (5)	21.9 (3)	0.732	0.278	0.07 (2)	0.72 (1)	1.31	1.505	0.909
HF(*A*,*U*)	2.27 (4)	20.8 (2)	0.677	0.335	0.07 (1)	0.65 (1)	1.31	1.516	0.908
HF(*A*,*U*,*S*)	2.02 (3)	19.6 (2)	0.727	0.284	0.06 (1)	0.61 (1)	1.14	1.558	0.937
HF(*A*,*U*,*D*)	2.25 (4)	20.8 (2)	0.690	0.321	0.02 (1)	0.82 (1)	1.03	1.648	0.928
HF(6-21G**,*A*,*U*)	2.20 (2)	21.5 (1)	0.716	0.294	0.05 (1)	0.05 (1)	1.36	1.495	0.904
BLYP(CMO)	2.39	33.7	0.706	0.304	0.04	0.94	1.23	1.498	0.923
BLYP(*L*,*W*)	2.23 (9)	22.5 (5)	0.710	0.301	0.08 (2)	0.81 (2)	1.51	1.452	0.946
BLYP(*L*,*U*)	2.26 (6)	20.4 (3)	0.693	0.319	0.07 (2)	0.67 (1)	1.32	1.482	0.933
BLYP(*A*,*W*)	2.20 (5)	21.9 (3)	0.708	0.303	0.08 (1)	0.79 (1)	1.52	1.461	0.938
BLYP(*A*,*W*,*S*)	1.98 (5)	20.5 (3)	0.748	0.262	0.07 (1)	0.74 (1)	1.33	1.495	0.918
BLYP(*A*,*U*)	2.24 (4)	21.0 (2)	0.697	0.314	0.07 (1)	0.64 (1)	1.30	1.503	0.929
BLYP(*A*,*U*,*S*)	1.99 (3)	20.1 (2)	0.743	0.268	0.06 (1)	0.67 (1)	1.15	1.540	0.952
BLYP(*A*,*U*,*D*)	2.24 (3)	21.3 (2)	0.708	0.302	0.03 (1)	0.94 (1)	1.16	1.606	0.895
EXP(*L*,*W*,*D*)	2.10 (1)	18.46 (1)	0.727	0.283	0.03 (1)	1.03 (1)	1.20	1.578	0.851

Abramov, Coppens & Gatti, 2000; Volkov, Gatti, Abramov & Coppens, 2000).

Agreement statistics, multipole parameters, κ and κ' values are given in Tables 1 and 2.

The agreement factor R_f is given by

$$R_f = \frac{\sum_{i=1}^{n} \| F_i^{\rm obs}| - |F_i^{\rm mul} \|}{\sum_{i=1}^{n} |F_i^{\rm obs}|} \times 100\%,$$

where $F_i^{\rm mul}$ are the corresponding structure factors from the multipole refinement of the data $F_i^{\rm obs}$.

The following labelling scheme is used to distinguish between the different *XD* refinements and specifies the data and multipole models used in each analysis.

- HF, BLYP, EXP denote that the $F_i^{\rm obs}$ were obtained from either the HF or BLYP calculations using *CRYSTAL98* or from the experimental data of Boese *et al.* (1997).
- CMO denotes parameters obtained directly from the CMO wavefunction with no multipole refinement involved.
- *L* or *A* denotes the use of $(\sin\theta/\lambda) < 0.7$ Å^{-1} or $(\sin\theta/\lambda) < 1.05$ Å^{-1} data, respectively.
- *U* or *W* refers to the use of $\sigma(F_i^{\rm obs}) = 0.001$ or derived from the experimental data set, respectively.
- *S* is used to indicate the use of the Stewart *et al.* (1965) scattering factors for hydrogen with $\kappa({\rm H}) = \kappa'({\rm H}) = 1.16$. Otherwise, $\kappa({\rm H}) = \kappa'({\rm H}) = 1.2$ and the atomic hydrogen radial function was used.
- *D* denotes the use of only dipoles on H atoms.

Thus, HF(CMO) denotes values derived directly from a CMO Hartree–Fock calculation. Likewise, BLYP(*A*,*U*,*S*) refers to parameters from a multipole refinement of the structure factors obtained from a BLYP(CMO) calculation, using σ = 0.001 and Stewart *et al.* (1965) scattering factors for H.

3. Theoretical charge density

The theory of atoms in molecules (Bader, 1990) is well suited to the comparison of charge densities. Topological analyses of the charge density in order to find the lines of maximum density connecting nuclei (*i.e.* bond paths) and the associated point of minimum density along this line (*i.e.* the bond critical points) provide convenient measures of the differences between calculated and experimental charge densities.

The topology of the charge density for a single NH_3 molecule is relatively simple and consists of three bond critical points and associated bond paths, corresponding to each of the three N—H bonds. The bond critical point data for the N—H bond obtained from the present calculations are given in Table 3.

Previous theoretical studies of NH_3 using a variety of quantum-chemical methods show the N—H bond to be characterized by a bond critical point situated approximately 0.25 Å from the H nucleus with values of $\rho(\mathbf{r})$ and $-\nabla^2\rho(\mathbf{r}_b)$ of approximately 2.3 e Å^{-3} and 35 e Å^{-5}, respectively (Wang *et al.*, 1996). The values obtained from the CMO methods used here are similar [see HF(CMO) and BLYP(CMO) in Table 3].

The presence of a sterically active lone pair of electrons is fundamental to understanding the pyramidal stereochemistry of NH_3 (Gillespie & Hargittai, 1991). Pairs of electrons are not, however, apparent in a total charge density. However, the Laplacian of the charge density [$L = -\nabla^2\rho(\mathbf{r})$] shows where charge density is locally concentrated ($L > 0$) or depleted ($L < 0$), and the arrangement of critical points in L in the valence shell of an atom is its atomic graph (Bader, 1990). The correspondence between the location of charge concentration maxima [*i.e.* (3,−3) critical points] in L and electron pairs is well documented for main-group molecules (Bader *et al.*, 1988; Gillespie & Robinson, 1996). In particular, this observation

allows electron pairs to be re-defined as regions where charge is locally concentrated. Consequently, L may be used to locate electron density characterizing bonds and lone pairs. It provides a tool for gauging differences in charge densities and will be used here to help characterize the total electron density in NH_3.

The atomic graph of nitrogen obtained from the HF(CMO) charge density does not show the expected quasitetrahedral arrangement (Bader, 1990; Aray *et al.*, 1996; Gillespie & Robinson, 1996) of charge concentration maxima, *viz* one maximum along each N—H bond and one in the lone-pair region. Fig. 2(*a*) is a plot of L obtained from the HF(CMO) calculation and shows two charge concentration maxima: one in the 'lone-pair' region and one in the region 'anti' to this. The charge-concentration maxima expected along the N—H bonds are absent, reminiscent of the atomic graphs observed for some amine molecules (Aray *et al.*, 1996). The BLYP(CMO) calculation shows the same features.

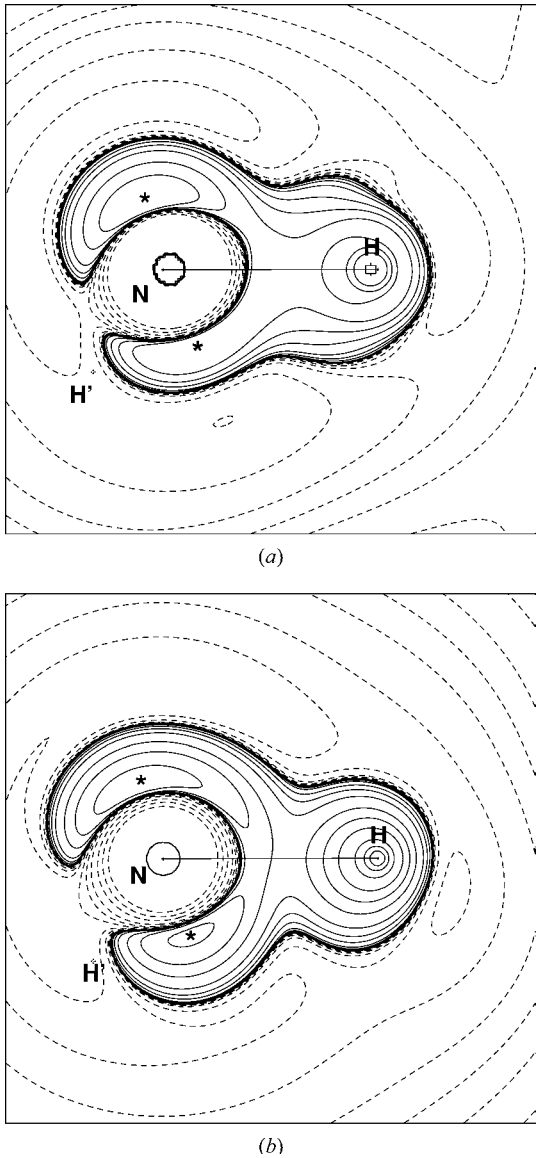

Figure 2
Plots of L obtained from (*a*) the HF(CMO) calculation and (*b*) the HF(A,U) refinement. Contours are drawn at intervals of (±2, ±4, ±8) $\times$ 10^n e Å^{-3} (n = -3 to $+3$). Full lines denote regions of charge concentration ($L > 0$) and broken lines denote regions of charge depletion ($L < 0$). Stars ($\star$) mark the two charge concentration maxima on each plot.

In the crystalline phase, an important feature of the packing of NH_3 is the presence of intermolecular hydrogen-bonding interactions, and characterization of hydrogen-bonding interactions in terms of the total charge densities obtained from theory is well established (Bader & Essén, 1984; Cheeseman *et al.*, 1988; Popelier & Bader, 1992; Taylor *et al.*, 1995). More recently, experimental electron densities have been analysed for hydrogen-bonding interactions (Macchi *et al.*, 2000), and characterized in terms of λ_3, the positive curvature of $\rho(\mathbf{r})$ at the bond critical point (Espinosa *et al.*, 1999).

Previous work with density functional theory (DFT) has indicated that the BLYP functional is satisfactory for the treatment of hydrogen-bond interactions (Florián & Johnson, 1995; Novoa & Sosa, 1995; Han & Suhai, 1996; Pudzianowski, 1996). Both HF and DFT calculations yielded bond critical points corresponding to the intermolecular N···H bonds.

The N···H interaction can also be examined in terms of the positive curvature of $\rho(\mathbf{r})$ at the bond critical point. This approach has been used to examine the O···H hydrogen-bonding interactions in a variety of molecules (Espinosa *et al.*, 1999), and it is of interest to see how this property transfers to other hydrogen-bonding interactions, *vis a vis* N···H. The values of λ_3 obtained from the various calculations are given in Table 3 and show reasonable agreement with the values expected for O···H hydrogen bonds extrapolated to a similar internuclear separation [see Fig. 5 of Espinosa *et al.* (1999)].

4. Multipole refinements

4.1. General discussion

The R_f agreement values obtained after the final least-squares refinement cycle are given in Table 1 and the corresponding multipole population parameters in Table 2. The refinement procedure used here was applied to the low-angle experimental data set $(\sin\theta/\lambda) < 0.7$ Å^{-1} (Boese *et al.*, 1997). In this refinement of the experimental data, denoted EXP(L,W,D), isotropic extinction was also refined assuming a path length of 0.30 mm. The residuals are low (see Fig. 4) and the refinement yields agreement statistics similar to those obtained by Boese *et al.* (1997).

While the fit to the experimental data is good, fitting to the theoretical structure factors is less satisfactory as can be seen from the tabulated R_f values (Table 1). However, fitting the experimental data included more variables since it involved the refinement of thermal parameters. The use of equal weights (σ = 0.001) [HF(A,U) and BLYP(A,U)] rather than the experimental weights [HF(A,W) and BLYP(A,W)] leads to better agreement, and the use of the Stewart *et al.* hydrogen functions rather than the exact atomic hydrogen functions has only a slight effect, causing an improvement in one case

[BLYP(A,W,S)] and a worsening in all others. Use of the refinement scheme of Moss *et al.* (1995) without inclusion of positional or displacement parameters did not lead to any improvement in the agreement factor. The best fit to the theoretical data as measured by R_f comes from the model fitting the complete set of data ($\sin\theta/\lambda < 1.05$ Å^{-1} with equal weight given to all reflections, quadrupolar functions on H, and using the atomic radial function on H [HF(A,U) and BLYP(A,U)].

None of the models or strategies used was able to make an excellent fit in terms of R_f to the densities produced using the basis set chosen. A different density, however, was produced using the 6-21G basis (Binkley *et al.*, 1980), augmented by *d* and *p* polarization functions on N and H, respectively (Hariharan & Pople, 1973), and included with the *CRYSTAL98* software. This basis gives an atomic graph for N which conforms to that expected from an isolated ammonia molecule and does not have any maximum in L in the region opposite to the lone pair. This theoretical density can be much better fitted by the multipole model HF(A,U) ($R_f = 0.99$) than the densities obtained using the truncated 6-311G** basis.

The goodness of fit evidenced in the R_f values is confirmed by the residual density maps in Figs. 3 and 4. These plots are for the plane containing nitrogen, one hydrogen and the threefold axis; thus they pass through the centre of the region occupied by the lone pair. Refinement of the experimental data produced a residual plot with no substantial density in the sampling plane, indicating that the description of the electron density by the multipole fitting strategy used here is reasonable. Using the same strategy with the theoretical data leaves residual densities that do have features in this plane. Nevertheless, the electron density is still reasonably satisfactorily modelled since the highest magnitude of any residual feature in this plane is 0.34 e Å^{-3} for the model BLYP(A,U,D). All other residual densities have maximum features of less than 0.29 e Å^{-3} in magnitude (Fig. 4).

Features shown by the residual densities are quite distinctively related to the multipole model. If the model HF(A,U) is

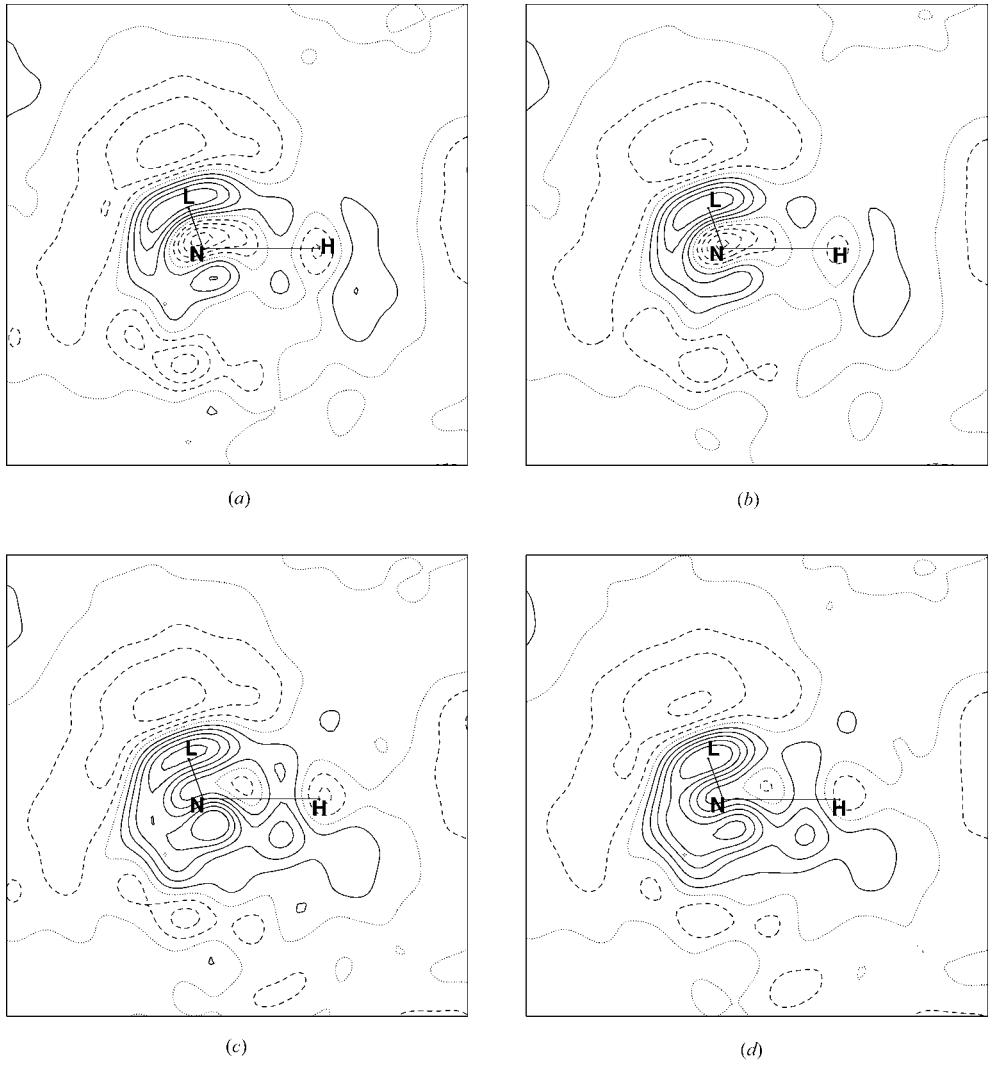

Figure 3
Residual plots for the various refinements. Contours are at 0.05 e Å^{-3} with full lines denoting positive contours, dashed lines negative contours, and the zero contour is denoted by the dotted line. (*a*) HF(A,U), (*b*) BLYP(A,U), (*c*) HF(A,W), (*d*) BLYP(A,W).

taken as a standard then changing to use of the experimental weights reduces the residue well around the N and increases the residual peak in the region of the lone-pair region and in the area opposite the lone pair. The most prominent result of using the Stewart *et al.* scattering factors for H is an increase in the residual well centred around H. Finally, having no more than dipolar functions on H has the effect of deepening the residue well around N, obliterating the feature centred on H, and slightly decreasing the residue features around the N. Despite the lower R_f value for the HF(A,U) refinement of the data from the 6-21G** basis, the residual map from this analysis still has evident features. However, they are somewhat lower in magnitude than those in the residual maps from the larger basis set, the largest residue being 0.17 e Å^{-3} (see Fig. 4).

Further discussion will concentrate on examining the results from the multipole model that best fits the theoretical data for each of the HF and BLYP calculations. These are the results HF(A,U) and BLYP(A,U).

4.2. The N—H bond

Details of the bond critical points are given in Table 3, which contains information about the charge densities from the theoretical calculations and after multipole analysis. The position of the N—H bond critical point is reproduced by the best analyses HF(A,U) and BLYP(A,U) with an accuracy of 10%, based on the distance from H. There is little variation in the positioning of this critical point with the refinement model used. The only variation of note is that use of the Stewart *et al.* H scattering factors resulted in the critical point being located closer to the H than the theoretical density, whereas the atomic radial function for H consistently places it farther from H. The use of quadrupoles on H does not make a significant difference.

The charge density at the N—H bond critical point $\rho(\mathbf{r}_b)$ is reproduced to within 7% for the best fit results. Other multipole models are very close to this except when the Stewart *et al.* H functions are used, in which case $\rho(\mathbf{r}_b)$ is lower and farther from agreement with the reference density.

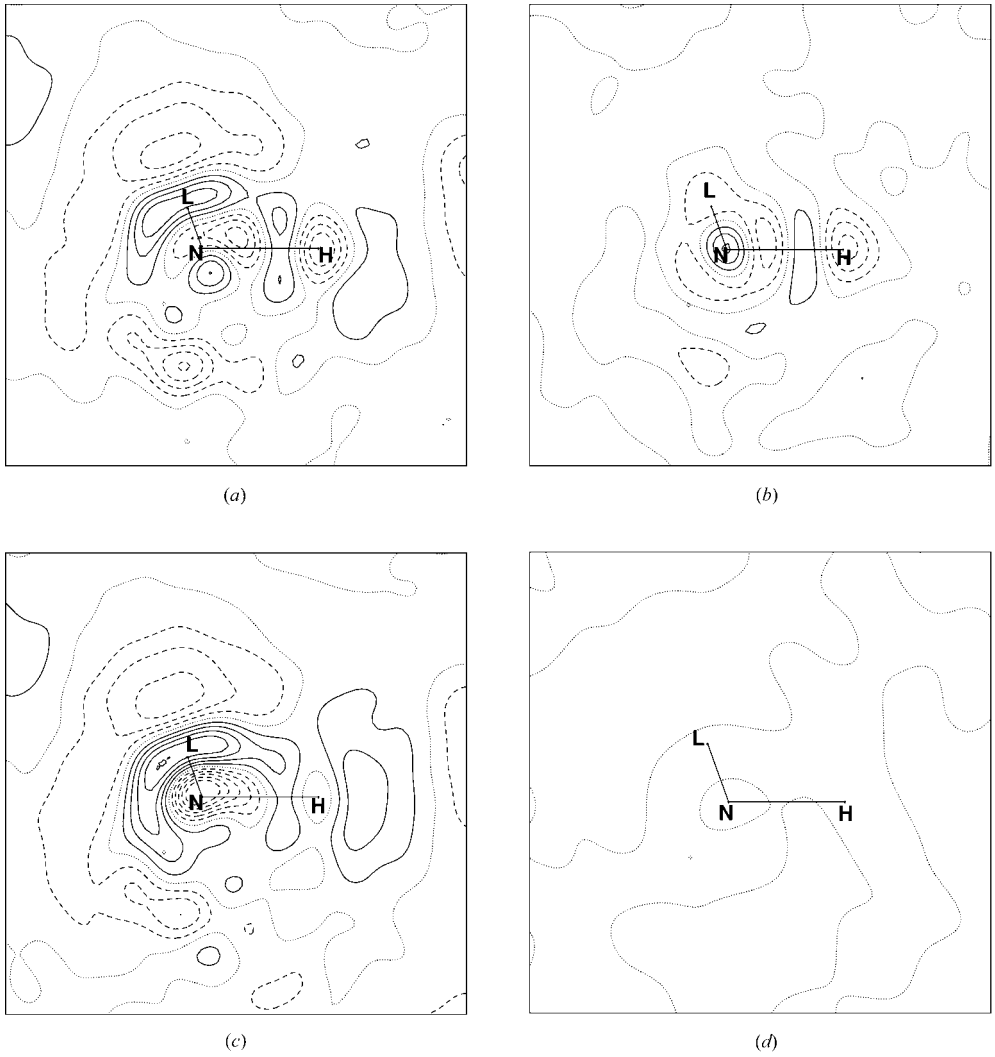

Figure 4
Residual plots for the various refinements. Contours are at 0.05 e Å^{-3} with full lines denoting positive contours, dashed lines negative contours, and the zero contour is denoted by the dotted line. (*a*) HF(A,U,S), (*b*) HF(621G**,A,U), (*c*) HF(A,U,D), (*d*) EXP(L,W,D).

Table 4
Parameters for the atomic graph of nitrogen obtained from the CMO calculations and the *XD* refinements .

L (e Å^{-5}) is the value for the charge concentration maximum at the (3,−3) critical point and d(N) (Å) is its distance from the nitrogen nucleus.

	Lone pair (3,−3)		Anti (3,−3)	
Data	L	d(N)	L	d(N)
HF(CMO)	180.44	0.363	48.39	0.415
HF(L,W)	119.68 (7)	0.369	87.03 (6)	0.385
HF(L,U)	119.0 (3)	0.367	105.5 (3)	0.379
HF(A,W)	127.41 (4)	0.370	79.51 (4)	0.380
HF(A,W,S)	137.85 (4)	0.369	83.60 (4)	0.386
HF(A,U)	122.79 (4)	0.368	94.73 (4)	0.383
HF(A,U,S)	134.72 (4)	0.367	93.65 (5)	0.383
HF(A,U,D)	128.59 (4)	0.369	88.07 (4)	0.383
HF(6-21G**,A,U)	64.02 (1)	0.398	49.82 (2)	0.405
BLYP(CMO)	138.45	0.370	57.62	0.410
BLYP(L,W)	93.60 (9)	0.377	83.03 (8)	0.385
BLYP(L,U)	88.4 (1)	0.374	109.9 (1)	0.378
BLYP(A,W)	93.71 (3)	0.377	84.55 (4)	0.386
BLYP(A,W,S)	105.90 (4)	0.376	91.28 (4)	0.385
BLYP(A,U)	93.09 (4)	0.376	94.70 (4)	0.381
BLYP(A,U,S)	107.56 (4)	0.373	95.75 (4)	0.381
BLYP(A,U,D)	97.78 (3)	0.376	87.32 (3)	0.383
EXP(L,W,D)	41.97 (1)	0.414	40.24 (1)	0.414

$\nabla^2\rho(\mathbf{r}_b)$ is more difficult to reproduce. For ammonia, multipole analysis significantly reduces the magnitude of $\nabla^2\rho(\mathbf{r}_b)$ for both bond critical points and charge concentration maxima (see Tables 3 and 4). The extreme variability in this parameter arises because $\nabla^2\rho(\mathbf{r})$ is a second derivative giving the rate of change of the slope of the charge density, which is a matter of fine detail in the surface, and difficult to estimate. This sensitivity has been noted before by Pérès *et al.* (1999). For the N—H bond, the reduction is 58 and 38% for HF(A,U) and BLYP(A,U), respectively. Other models do not differ markedly from this.

4.3. The intermolecular N···H bond

Bond parameters for the N···H bond are given in Table 3. The multipole models differ considerably in their ability to deal with the two reference charge densities in reproducing the position of the N···H bond critical point relative to the nuclei. HF(A,U), and all other models operating on the HF density, locate this critical point closer to the H than in the starting charge density. The error is only 12% but since the bond length is large this translates to a sizeable absolute value. By contrast, BLYP(A,U) results in very accurate positioning of the N···H bond critical point in relation to its reference density. The other bond parameters, $\rho(\mathbf{r}_b)$ and $-\nabla^2\rho(\mathbf{r}_b)$, are small for this weak bond and both are very satisfactorily reproduced by the multipole models. The fact that multipole models do not give a large variablity in $\nabla^2\rho(\mathbf{r}_b)$ values when $\rho(\mathbf{r}_b)$ and $\nabla^2\rho(\mathbf{r}_b)$ are small has been noted before by Pérès *et al.* (1999).

4.4. Non-bonded charge concentrations

Even though the atomic graphs given by the CMO densities are unexpected, multipole refinement faithfully reproduces the atomic graphs of the starting densities. This is true for the density from the truncated 6-311G** basis, with its atomic graph containing a critical point opposite to the N lone-pair region, and also for the density from the 6-21G** basis which does not have a critical point opposite the N lone-pair region.

The topological parameters for the critical points associated with charge concentrations that are not associated with bonds are given in Table 4. For the theoretical densities under consideration, there are two such points. One is associated with the lone-pair region and the other is associated with a region opposite the lone pair. The *XD*-generated plots of L appear similar to the original CMO plot (see Fig. 2) and the distance of the lone-pair critical point from N is well reproduced by the multipole analysis. This is not true for L which for HF(A,U) and BLYP(A,U) is lowered by 32 and 33%, respectively. Similarly large errors come from all the refinement models used in this study. With the charge concentration opposite the lone-pair region, there is an opposite effect; L is raised by the multipole refinement with HF(A,U) and BLYP(A,U) giving errors in L of 96 and 64%, respectively.

5. Conclusions

Topological analysis of total charge densities obtained from crystalline *ab initio* (CMO) calculations and from multipole refinement of X-ray structure factors generated from the same calculation has provided a method of testing the ability of multipolar density functions to reproduce a known charge density. While the multipole refinement strategies used here sampled most of the charge density carried by the experimental X-ray structure factors, they could not do as well with theoretical structure factors. This is clearly shown by the R_f factors and in residual plots. The ability to reproduce a charge density is connected to the actual reference charge density, so that the CMO electron density produced from a 6-21G** basis is better reproduced than that from the density from a truncated 6-31G** basis. The limited experimental data set is better fitted than any of the theoretical charge densities, although it should be noted that this fit also involved refinement of thermal parameters. In this work, the use of the scaled Stewart *et al.* scattering factors for H did not improve the multipole fit as compared to use of the scaled atomic H radial function.

We thank Dr A. N. Sobolev, Dr V. Streltsov and Professor M. A. Spackman for helpful discussions concerning multipole refinement strategies and Dr C. Gatti for providing a copy of the *TOPOND* program. Financial support from the Australian Research Council is gratefully acknowledged.

References

Abramov, Y. A., Volkov, A. & Coppens, P. (1999). *Chem. Phys. Lett.* **311**, 81–86.
Aray, Y., Casilamas, J. C. & Murgich, J. (1996). *J. Phys. Chem.* **100**, 5291–5298.
Bader, R. F. W. (1990). *Atoms in Molecules: a Quantum Theory.* Oxford University Press.

Bader, R. F. W. & Essén, H. (1984). *J. Chem. Phys.* **80**, 1943–1960.
Bader, R. F. W., MacDougall, P. J. & Gillespie, R. J. (1988). *J. Am. Chem. Soc.* **110**, 7329–7336.
Becke, A. D. (1988). *Phys. Rev.* A**38**, 3098–3100.
Bentley, J. J. & Stewart, R. F. (1976). *Acta Cryst.* A**32**, 910–914.
Bianchi, R., Gervasio, G. & Marabello, D. (2000). *Inorg. Chem.* **39**, 2360–2366.
Binkley, J. S., Pople, J. A. & Hehre, W. J. (1980). *J. Am. Chem. Soc.* **102**, 939–947.
Boese, R., Niederprüm, N., Bläser, D., Maulitz, A., Antipin, M. & Mallinson, P. R. (1997). *J. Phys. Chem.* B**101**, 5794–5799.
Bytheway, I., Figgis, B. N. & Sobolev, A. N. (2001). *J. Chem. Soc. Dalton Trans.* pp. 3285–3294.
Cheeseman, J. R., Carroll, M. T. & Bader, R. F. W. (1988). *Chem. Phys. Lett.* **143**, 450–458.
Clementi, E. & Raimondi, D. L. (1963). *J. Chem. Phys.* **38**, 2686–2689.
Clementi, E. & Roetti, C. (1974). *At. Data Nucl. Data Tables*, **14**, 177–478.
Coppens, P. (1992). *Annu. Rev. Phys. Chem.* **43**, 663–692.
Coppens, P. (1997). *X-ray Charge Densities and Chemical Bonding.* New York: Oxford University Press.
Dawson, B. (1967). *Proc. R. Soc. London Ser. A*, **298**, 255–263.
Dovesi, R., Saunders, V. R., Roetti, C., Causà, M., Harrison, N. M., Orlando, R. & Aprà, E. (1996). *CRYSTAL95 Users Manual.* University of Torino, Torino, Italy.
Epstein, J., Bentley, J. J. & Stewart, R. F. (1977). *J. Chem. Phys.* **66**, 5564–5567.
Espinosa, E., Souhassou, M., Lachekar, H. & Lecomte, C. (1999). *Acta Cryst.* B**55**, 563–572.
Flaig, R., Koritsánszky, T., Zobel, D. & Luger, P. (1998). *J. Am. Chem. Soc.* **120**, 2227–2238.
Florián, J. & Johnson, B. G. (1995). *J. Phys. Chem.* **99**, 5899–5908.
Gatti, C. (1998). *TOPOND.* CNR-CSRSRC, Milan, Italy.
Gillespie, R. J. & Hargittai, I. (1991). *The VSEPR Model of Molecular Geometry.* Boston: Allyn and Bacon.
Gillespie, R. J. & Robinson, E. A. (1996). *Angew. Chem. Int. Ed. Engl.* **35**, 495–514.
Han, W. G. & Suhai, S. (1996). *J. Phys. Chem.* **100**, 3942–3948.
Hariharan, P. C. & Pople, J. A. (1973). *Theor. Chim. Acta*, **28**, 213–222.
Howard, S. T., Hursthouse, M. B., Lehmann, C. W., Mallinson, P. R. & Frampton, C. S. (1992). *J. Chem. Phys.* **97**, 5616–5630.
Howard, S. T., Hursthouse, M. B., Lehmann, C. W. & Poyner, E. A. (1995). *Acta Cryst.* B**51**, 328–337.
Iversen, B. B., Larsen, F. K., Figgis, B. N. & Reynolds, P. (1997). *J. Chem. Soc. Dalton Trans.* pp. 2227–2240.
Koritsánszky, T., Howard, S. T., Su, Z., Mallinson, P. R., Richter, T. & Hansen, N. (1997). *XD, Computer Program Package for Multipole Refinement and Analysis of Electron Densities from Diffraction Data.* Free University of Berlin, Berlin, Germany.
Koritsánszky, T., Buschmann, J., Lentz, D., Luger, P., Perpetua, G. & Röttger, M. (1999). *Chem. Eur. J.* **5**, 3413–3420.
Koritsánszky, T. & Coppens, P. (2001). *Chem. Rev.* **101**, 1583–1627.
Koritsánszky, T., Zobel, D. & Luger, P. (2000). *J. Phys. Chem.* A**104**, 1549–1556.
Krishnan, R., Binkley, J. S., Seeger, R. & Pople, J. A. (1980). *J. Chem. Phys.* **72**, 650–654.
Lee, C., Yang, W. & Parr, R. G. (1988). *Phys. Rev. B*, **37**, 785–789.
Lippmann, T. & Schneider, J. R. (2000). *Acta Cryst.* A**56**, 575–584.
Macchi, P., Iversen, B. B., Sironi, A., Chakoumakos, B. C. & Larsen, F. K. (2000). *Angew. Chem. Int. Ed. Engl.* **39**, 2719–2722.
Macchi, P., Proserpio, D. M. & Sironi, A. (1998*a*). *J. Am. Chem. Soc.* **120**, 13429–13435.
Macchi, P., Proserpio, D. M. & Sironi, A. (1998*b*). *J. Am. Chem. Soc.* **120**, 1447–1455.
Moss, G. R., Souhassou, M., Blessing, R. H., Espinosa, E. & Lecomte, C. (1995). *Acta Cryst.* B**51**, 650–660.
Novoa, J. J. & Sosa, C. (1995). *J. Phys. Chem.* **99**, 15837–15845.
Pérès, N., Boukhris, A., Souhassou, M. & Lecomte, C. (1999). *Acta Cryst.* A**55**, 1038–1048.
Pillet, S., Souhassou, M., Lecomte, C., Schwarz, K., Blaha, P., Rérat, M., Lichanot, A. & Roversi, P. (2001). *Acta Cryst.* A**57**, 290–303.
Popelier, P. L. A. & Bader, R. F. W. (1992). *Chem. Phys. Lett.* **189**, 542–548.
Pudzianowski, A. (1996). *J. Phys. Chem.* **100**, 4781–4789.
Rosso, K. M., Gibbs, G. V. & Boisen, M. B. (1999). *Phys. Chem. Miner.* **26**, 264–272.
Saunders, V. R., Dovesi, R., Roetti, C., Causà, M., Harrison, N. M., Orlando, R. & Zicovich-Wilson, C. M. (1998). *CRYSTAL98 Users Manual.* University of Torino, Torino, Italy.
Smith, G. T., Mallinson, P. R., Frampton, C. S., Farrugia, L. J., Peacock, R. D. & Howard, J. K. (1997). *J. Am. Chem. Soc.* **119**, 5028–5034.
Souhassou, M. & Blessing, R. H. (1999). *J. Appl. Cryst.* **32**, 210–217.
Spackman, M. A. & Byrom, P. G. (1996). *Acta Cryst.* B**52**, 1023–1035.
Spackman, M. A., Byrom, P. G., Alfredsson, M. & Hermansson, K. (1999). *Acta Cryst.* A**55**, 30–47.
Stewart, R. F. (1976). *Acta Cryst.* A**32**, 565–574.
Stewart, R. F., Davidson, E. R. & Simpson, W. T. (1965). *J. Chem. Phys.* **42**, 3175–3187.
Taylor, D. K., Bytheway, I., Barton, D. H. R., Bayse, C. A. & Hall, M. B. (1995). *J. Org. Chem.* **60**, 435–444.
Volkov, A., Abramov, Y. A. & Coppens, P. (2001). *Acta Cryst.* A**57**, 272–282.
Volkov, A., Abramov, Y., Coppens, P. & Gatti, C. (2000). *Acta Cryst.* A**56**, 332–339.
Volkov, A., Gatti, C., Abramov, Y. & Coppens, P. (2000). *Acta Cryst.* A**56**, 252–258.
Vries, R. Y. de, Feil, D. & Tsirelson, V. G. (2000). *Acta Cryst.* B**56**, 118–123.
Wang, J., Johnson, B. G., Boyd, R. J. & Eriksson, L. A. (1996). *J. Phys. Chem.* **100**, 6317–6324.